Journal of Statistical Physics, Vol. 64, Nos. 5/6, 1991

Dispersive Chaos

James A. Glazier,[1] Paul Kolodner,[1] and Hugh Williams[1]

"Dispersive chaos" refers to a dynamical state in which repetitive pulsing caused by strong nonlinear dispersion produces continuously erratic spatiotemporal behavior. We have observed this behavior in experiments on one-dimensional traveling-wave convection in an annular container. Based on measured physical parameters, this system can be modeled by a complex Ginzburg–Landau equation in the limit of strong nonlinear dispersion. The experimental observations are reminiscent of numerical simulations in this limit.

KEY WORDS: Traveling-wave convection; nonlinear dispersion; Ginzburg–Landau equation.

In this paper, we report experimental observations of dynamical states of weakly nonlinear, one-dimensional traveling-wave (TW) convection in annular containers. These states are strikingly different from those seen in rectangular containers. In a rectangular geometry, nonlinear competition between counterpropagating waves, which is enforced by the presence of reflections from the endwalls of the cell, dominates the dynamics. This competition leads to a regular alternation of wave energy between the two oppositely-propagating wave components that has been called "blinking" or "sloshing."[1] In annular containers, there are no such reflections, and it is possible to create a unidirectional TW state. However, even in the absence of a counterpropating wave, there is no stable, saturated weakly nonlinear state in an annular container. Instead, we observe a continuously erratic dynamical state in which the repetitive formation and abrupt collapse of narrow spatiotemporal pulses is characteristic. By measuring the physical parameters of the system and comparing our results with numerical simulations of the complex Ginzburg–Landau equation in the same parameter limit, we can identify the cause of this behavior as strong

[1] AT & T Bell Laboratories, Murray Hill, New Jersey 07974-2070.

822/64/5-6-4

0022-4715/91/0900-0945$06.50/0 © 1991 Plenum Publishing Corporation

nonlinear dispersion. We thus refer to this dynamical state as "dispersive chaos."

The characteristics of this physical system and the experimental techniques we use to study it have been described in several recent publications.[1–3] For appropriate parameters, a thin, horizontal layer of a binary fluid which is heated from below suffers an instability to traveling waves.[4] Just above the onset of this instability, a variety of nonlinear states can occur. The principal control parameter is the Rayleigh number R, which is proportional to the temperature difference applied vertically across the layer. The onset of the oscillatory instability is denoted R_{co}. In this paper, we quote the fractional distance above the onset of convection, defined as $\varepsilon \equiv (R - R_{co})/R_{co}$. The most important thermodynamic property of the fluid is its separation ratio ψ, which measures the influence of Soret-induced concentration diffusion on the stratification of density across the layer. The experiments reported in this paper employed ethanol/water mixtures with separation ratios[5] $\psi = -0.021$, -0.041, -0.050, and -0.069.

The convection containers consist of narrow channels in plastic plates clamped between a mirror-polished bottom plate and a transparent top plate. Cooling water circulates over the top plate, and the bottom plate is heated electrically. We visualize the convection patterns by shadowgraphy from above.[3] The patterns are always one-dimensional, consisting of superpositions of waves which propagate in opposite directions parallel to the long dimension of the cell. We denote the two directions of wave propagation by "left" and "right." The spatial profiles of the oppositely-propagating wave amplitudes are calculated as functions of time using complex demodulation of data acquired by an annular camera which views the shadowgraph image.[3]

The procedure we use in these experiments is similar to that reported previously.[1–3] We begin by determining the onset of convection. First, the temperature difference ΔT applied vertically across the cell is increased in small jumps until oscillations caused by the linear TW instability are observed. Then, the computer which controls the annular camera begins computing a wave-amplitude signal, which is set equal to the sum of the spatially-integrated left- and right-wave amplitude profiles calculated using complex demodulation. The temperature difference ΔT is then adjusted periodically to keep the wave-amplitude signal constant. This system servos the cell at the convective threshold of the linear instability, defining $\varepsilon \equiv 0$. Once the onset has been accurately measured, the servo is disabled, ε is increased to some desired value, and the dynamical evolution at constant ε is observed.

In rectangular cells, the first nonlinear state seen upon raising the

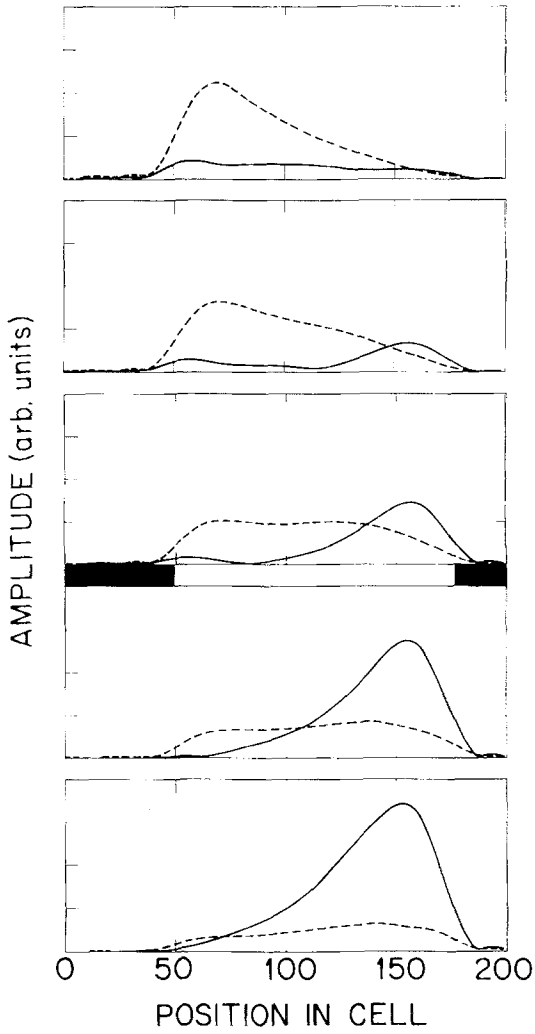

Fig. 1. Spatiotemporal behavior in a "blinking" state created at $\varepsilon = 3 \times 10^{-4}$ in a rectangular container, with $\psi = -0.021$. In each frame, the amplitudes of the left-going (dashed curves) and right-going (full curves) wave components at a particular time are plotted as functions of position of the cell, whose edges are delimited by the black horizontal bars. Time proceeds upward, and the entire figure covers one-half of a blinking cycle. The blinking consists of a periodic exchange of wave amplitude between the two wave components.

Rayleigh number to within a narrow range above onset consists of "blinking": wave energy oscillates slowly back and forth across the cell.[1] Figure 1 shows an example of the demodulated wave profiles in this state. Cross[6] has seen remarkably similar behavior in numerical simulations of coupled Ginzburg–Landau equations with real coefficients. The cause of the blinking is the saturating nonlinear competition between oppositely-propagating wave components, represented in the equations by cubic cross-terms. The presence of one wave component tends to suppress the amplitude of the other. However, reflection of the dominant component from the endwall of the cell continues to feed energy into the suppressed component, which gradually grows until the roles of the two components reverse. This leads to slow oscillations on a time scale whose experimental dependence on ε can also be understood in the context of coupled Ginzburg–Landau equations using marginal-stability arguments.[7]

In an annular container, reflections of TW are weak, since they can only be caused by imperfections in the cell. It is therefore possible to create a unidirectional TW state.[8] Figure 2 shows that the evolution of such a state following a jump to slightly above the onset of convection consists in the formation of a spatially-localized pulse which then collapses abruptly. This dynamical event is independent of the state of the opposite wave component. Between the times of its formation and collapse, the pulse is observed to propagate at a roughly constant velocity s which is substantially lower than the group velocity of the linearly unstable waves seen at onset. As shown in Fig. 3, the subsequent evolution of a unidirectional state consists in repeated pulsing, at apparently random places in the cell, with little or no excitation of the opposite wave component. Similar behavior occurs in runs in which the two wave components start with comparable amplitudes (Fig. 4).

Figure 5 shows the time history of the spatially-averaged wave amplitudes in an initially left-going state. Wave energy builds up only slowly in the right-wave component, indicating that reflections or nonlinear interactions between the two waves are weak. At later times, the spatially-averaged wave amplitudes in the resulting bidirectional state exhibit some correlation in time, but little in space. The two wave components appear to evolve independently.

The key to the origin of this erratic, repetitive pulsing behavior lies in the roles of nonlinear damping and dispersion, as represented by the real and imaginary parts of the cubic coefficient in a complex Ginzburg–Landau model for the amplitude of a unidirectional TW state:[9]

$$\frac{\partial A}{\partial t} + s\frac{\partial A}{\partial x} = A + (1 + ic_1)\frac{\partial^2 A}{\partial x^2} - g(1 + ic_2)|A|^2 A \tag{1}$$

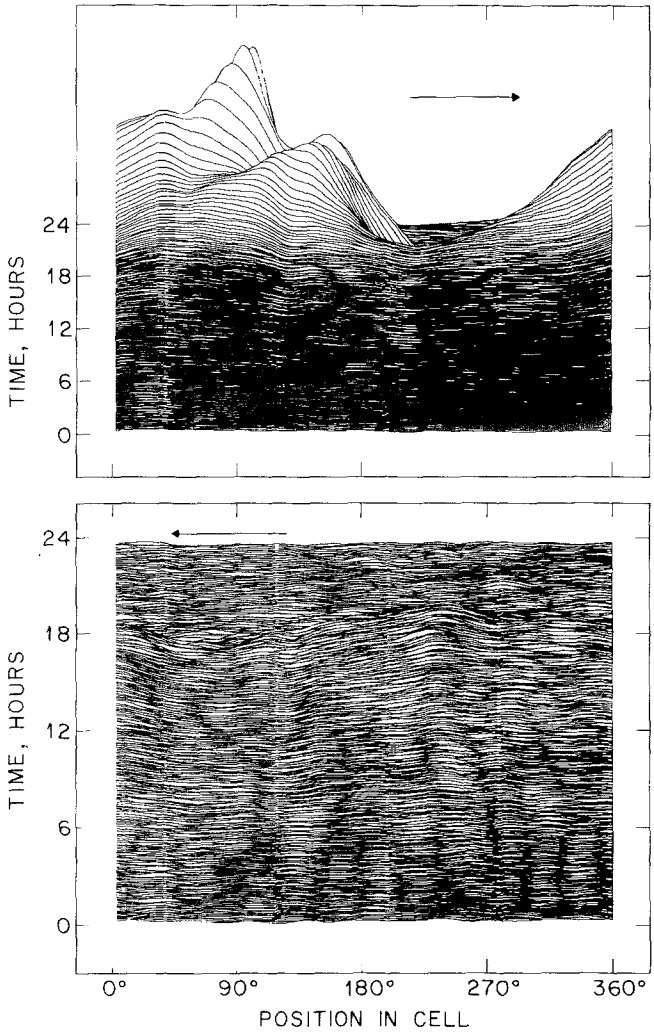

Fig. 2. Hidden-line plots showing the spatiotemporal behavior of the right-going (top) and left-going (bottom) wave amplitude profiles in an annular cell, with $\psi = -0.021$, following a jump in the Rayleigh number from just below the onset of the TW instability (at $\varepsilon \equiv 0$) to just above ($\varepsilon = 2.4 \times 10^{-4}$). The traces in these plots show the wave amplitude as a function of position at subsequent times, with time proceeding upward. An initial, nearly-uniform, small-amplitude, unidirectional state of linear waves grows up into a double-humped spatial pulse which fills about half the cell. This pulse later collapses everywhere in space and then grows up again somewhere else. The left-going wave component remained at zero amplitude during this run. After ref. 8.

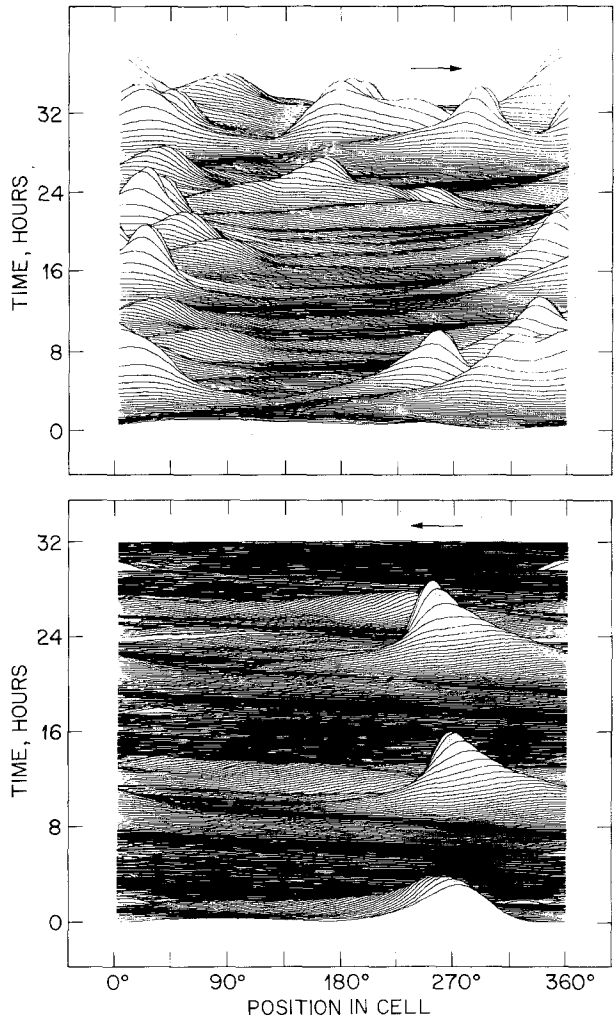

Fig. 3. Evolution of a nearly undirectional pulsing state at $\psi = -0.021$, at a higher Rayleigh number ($\varepsilon = 1.3 \times 10^{-3}$) than in the previous figure. The state of the right-wave component consists in repeated episodes of pulse formation and collapse at spatial locations which appear random. In contrast, the left-wave component exhibits only three isolated pulses.

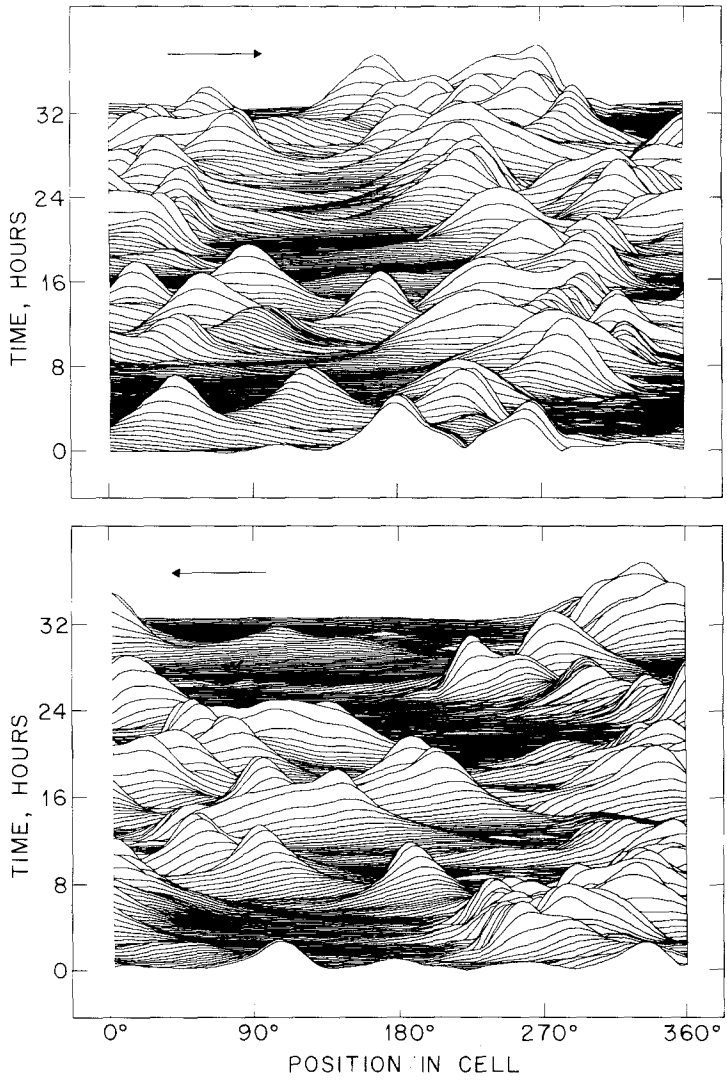

Fig. 4. Hidden-line plots showing the spatiotemporal behavior of the right (top) and left (bottom) wave components during a run at $\varepsilon = 5.9 \times 10^{-3}$, with $\psi = -0.021$. Both wave components exhibit a profusion of strongly localized pulses, and the evolutions of the two components appear to be independent. After ref. 8.

The scaling of this equation has been chosen so that $g = \pm 1$. Below, we show that $g = -1$. Higher-order nonlinear terms also appear to be negligible (see below). Because the two wave components evolve independently, we have not included in Eq. (1) any terms which represent their interaction.[6] Thus, this equation can be transformed into a comoving frame where the group velocity s vanishes.[2]

The linear dispersion coefficient c_1 has been calculated[10] and measured.[11] In all of our experiments, c_1 is quite small. As we detail below, we find erratic pulsing behavior with much in common with that described above for fluids with c_1 in the range -0.028 to $+0.022$. This suggests that, for small $|c_1|$, the sign of the linear dispersion is not important for the existence of this kind of dynamical behavior.

[2] The justification for transforming away the convective term in Eq. (1) is made somewhat subtle by the fact that the experiments are conducted above the threshold for the convective instability to linear TW, which propagate much faster than the pulse velocity s. However, immediately after the formation of a spatially-localized pulse in this system, the amplitude of fast, linear TW in the rest of the cell is quite small. The duration of the nonlinear pulses is short enough that the linear TW excited by noise in the rest of the system never have enough time to be amplified to observable amplitudes. Thus, the only important nonlinear dynamics in this system are those of the pulses themselves, for which there exists a unique, comoving frame.

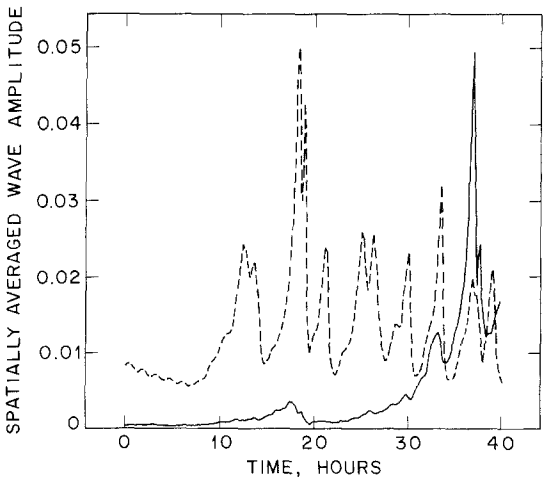

Fig. 5. Spatially-averaged right-wave (full curve) and left-wave (dashed curve) amplitudes plotted as functions of time during a run with $\psi = -0.041$. The Rayleigh number was raised from $\varepsilon = 0$ to $\varepsilon = 4.3 \times 10^{-4}$ at $t = 0$. Initially, all the wave amplitude was in the left component, but the right-wave component slowly grew to a comparable amplitude. The subsequent evolution of both components (not shown) was similar to that shown here for the left-going wave, with incomplete temporal correlation between the two waves.

We are also able to measure the nonlinear frequency-renormalization coefficient c_2 and compare our results with recent theoretical calculations. If we substitute a solution of the form

$$A(x, t) = \exp[(\gamma + i\Omega)t + (\lambda - i\Delta k)x] \tag{2}$$

into Eq. (1), we obtain $\gamma(A) = \gamma_0 - g|A|^2$ and $\Omega(A) = \Omega_0 - gc_2|A|^2$. Here, γ_0, the growth rate at infinitesimal amplitude, and Ω_0, the Hopf frequency, depend on the Rayleigh number, on the spatial growth rate λ, and on the wavenumber Δk. Thus, as a small-amplitude, unidirectional TW grows in amplitude above onset, its growth rate and frequency should exhibit quadratic dependences on the amplitude which in turn yield the sign of the coefficient g and the value of c_2. Figure 6 shows the shadowgraph light

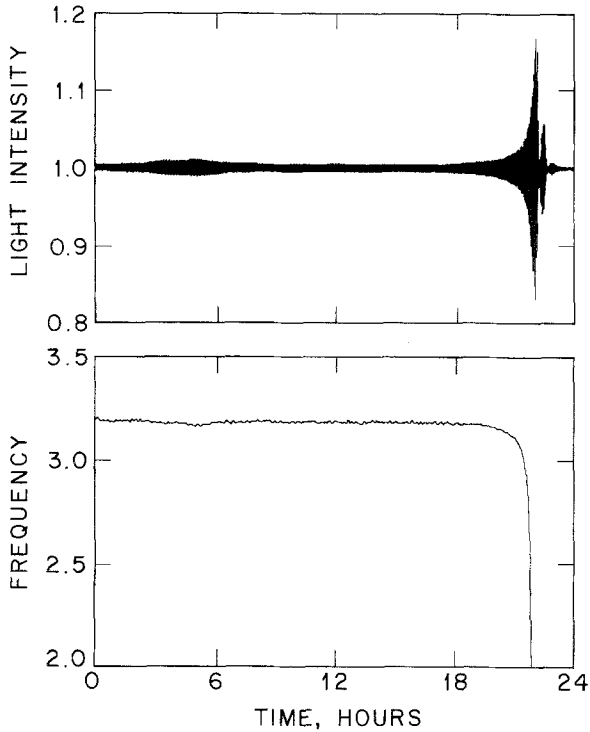

Fig. 6. The image intensity at a single spatial point (top) and its oscillation frequency (bottom) as functions of time during the growth of a unindirectional TW state with $\psi = -0.021$. Initially, the Rayleigh number was held near onset, so that the amplitude of the TW remained small. Then, at time $t = 17.5$ hours, the Rayleigh number was raised to $\varepsilon = 3 \times 10^{-4}$, resulting in a burst of amplitude and a drop in frequency due to nonlinear frequency renormalization.

intensity signal measured at a single spatial point during the growth near onset of such a state along with its oscillation frequency. Initially, the amplitude is small, and the oscillation frequency is equal to the Hopf frequency Ω_0. Then, after the Rayleigh number is increased, the frequency decreases abruptly as the amplitude grows into a pulse. In Fig. 7, we plot the growth rate and frequency as functions of the square of the oscillation amplitude. We find an approximately linear relationship for small amplitudes, as expected, and that $g = -1$. Averaging over several such measurements, the ratio of the slopes of linear fits to the two functions yields $c_2 = -7.2 \pm 1.5$ for $\psi = -0.021$. This is close to the theoretical result $c_2 = -9.84$.[12],[3]

The large magnitude of c_2 places our experiments firmly in the limit of strong nonlinear dispersion. Because $|c_2| \gg 1$, we suggest that these experiments can be modeled by neglecting the real part of the cubic term

[3] The calculated values for c_2 quoted here have been provided to us by W. Schöpf.

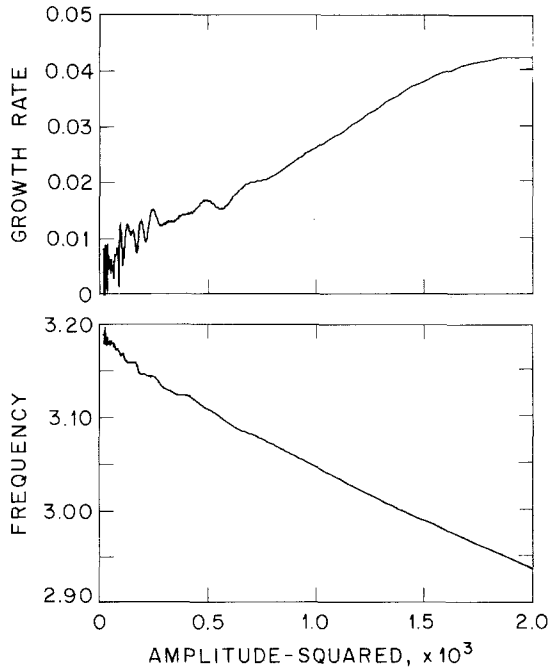

Fig. 7. The growth rate γ (top) and oscillation frequency Ω (bottom) as functions of the square of the signal amplitude for the data in Fig. 6. Both exhibit a component proportional to $|A|^2$, and the two slopes determine the sign of the saturation coefficient g and the value of the nonlinear frequency-renormalization coefficient c_2.

in Eq. (1), as well as higher-order nonlinear terms. Furthermore, because the data continue to exhibit erratic pulsing behavior when c_1 is changed from slightly positive to slightly negative (see below), we suggest that changing the sign of c_1 will not affect the applicability of Eq. (1) to this kind of dynamical state, for small $|c_1|$. If we then take the complex conjugate of Eq. (1), we arrive at the equation that was studied by Bretherton and Spiegel.[13] For $c_1 = 1$, these authors observed the same kind of pulsing behavior seen in our experiments. They argued that the reason for this pulsing is the strong nonlinear dispersion, which causes spatial nonuniformities to sharpen, and the absence of real nonlinear saturation, which causes the resulting pulses to grow to large amplitude before collapsing. Thus, the resulting state of continuously erratic pulsing can be called "dispersive chaos." The neglect of a destabilizing cubic nonlinearity and the assumption of very strong linear dispersion may seem inappropriate to our experiments. However, the large value of c_2 and the qualitative similarity of the dynamical states seen in these experiments to those in ref. 13 suggest that the experimental behavior is also caused by the strong nonlinear dispersion.

This interpretation has recently been put on a firmer basis by the work of Schöpf and Kramer,[14] who retained the destabilizing real part of the cubic term in Eq. (1) and numerically surveyed the dynamical behavior over a wide range of c_1 and c_2, including the region near $c_1 = 0$ in which we conducted these experiments. They found that, for sufficiently large $|c_2|$, nonlinear dispersion balances the destabilization and leads to the existence of bounded, chaotic solutions over a large region of (c_1, c_2) space. Below, we describe experiments in which we change the values of c_1 and c_2 by changing the experimental fluid. For values inside the bounded-chaotic region of ref. 14, we continue to observe erratic pulsing behavior. Outside this region, we observe a completely different behavior. On this basis, we claim that our results also exhibit "dispersive chaos." This behavior is not observed in rectangular containers, because of the strong damping due to the loss upon reflection of waves from the endwalls of the cell.[15]

For the separation ratio $\psi = -0.021$ at which most of the results exhibited so far were obtained, the linear dispersion coefficient $c_1 = +0.022$. As ψ is made more negative, c_1 passes through zero.[10] However, the more noteworthy parameter change is that c_2 becomes less negative.[12] Thus, by decreasing ψ, we expect at some point to arrive in a regime where nonlinear dispersion is no longer important. This crossover is indeed observed. Figure 8 shows the dynamics for $\psi = -0.041$ ($c_1 = -0.015$[10] and $c_2 = -7.39$[12]). For $\varepsilon \geqslant 1.7 \times 10^{-3}$, the amplitude peaks are strongly isolated in space and time and are much stronger than the background. We could characterize this state as one in which large fractions of the cell are

inactive for long times, while the state in Fig. 4 is one in which most of the cell is active most of the time. Alternatively, the state in Fig. 8 could be described as exhibiting an essentially bimodal pulse-height distribution, because a substantial fraction of spacetime is filled with "peaks" of zero height. In Fig. 4, the peak-height distribution is more nearly unimodal, since most of the cell is nearly always filled with peaks having a similar height. States of this "unimodal" type have also been observed for $\psi = -0.041$, at $\varepsilon = 1.1 \times 10^{-3}$ and $\varepsilon = 1.2 \times 10^{-3}$.

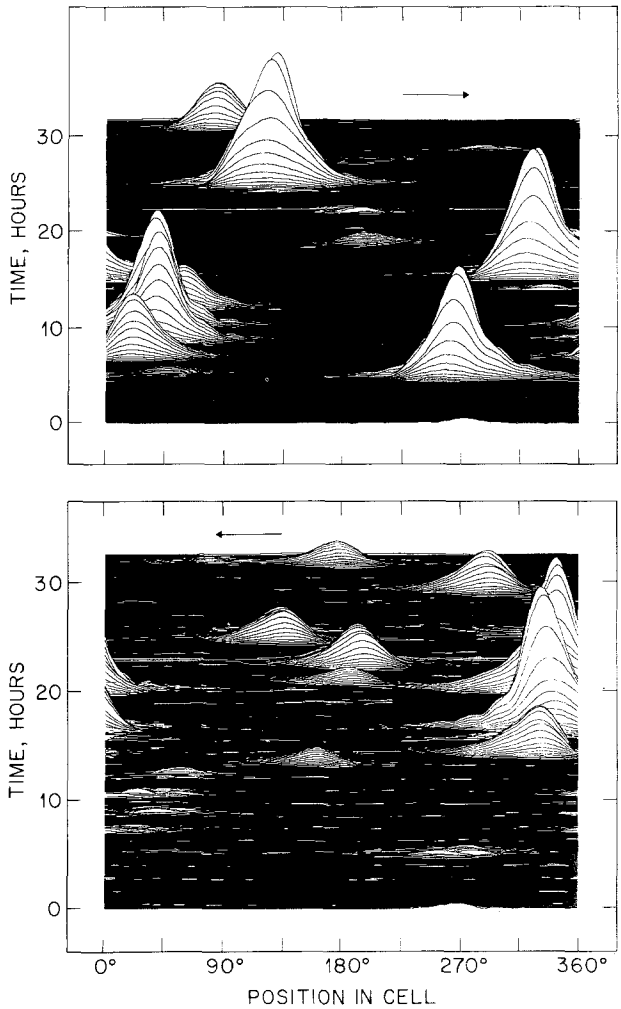

Fig. 8. Spatiotemporal behavior of a dispersively chaotic state in a fluid with $\psi = -0.041$, at $\varepsilon = 1.7 \times 10^{-3}$. Sharp, isolated peaks are seen in both wave components at this and higher ε.

For larger $|\psi|$ ($\psi = -0.050$, $c_1 = -0.028$, $c_2 = -6.69$), we again see erratic states which resemble those in Figs. 4 and 8. We have also seen the state shown in Fig. 9, which exhibits a rather broad distribution of peak heights.

We have not conducted a systematic exploration of nature of the dynamical states possible at all value of ε and ψ. However, we can make some general statements. First, while there are some qualitative differences

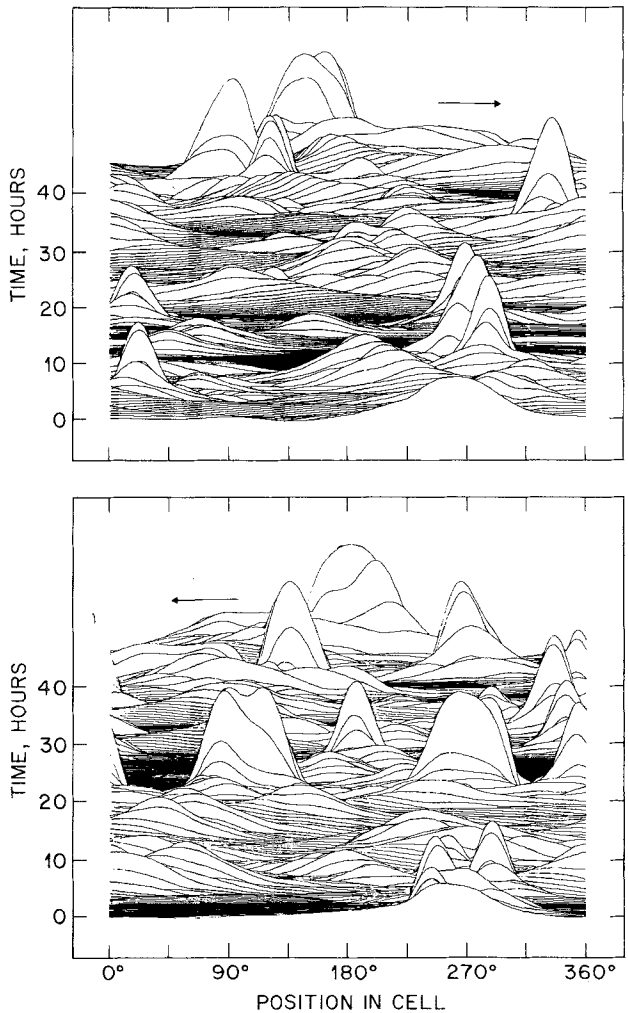

Fig. 9. Spatiotemporal behavior of a dispersively chaotic state at $\varepsilon = 1.8 \times 10^{-3}$, with $\psi = -0.050$. Tall, broad peaks, some with double humps, coexist with a low-intensity background.

between the dynamical states seen at different ψ, it should be stressed that they all exhibit the same basic "pulse-and-collapse" scenario caused by strong nonlinear dispersion. The qualitative changes between the states seen at different ψ may be related to the change of the sign of c_1.[14] Second, states exhibiting a unimodal distribution, like that in Fig. 4, have been seen at all three values of ψ. Third, it is possible to obtain different states at the same value of ψ and ε. For example, at $\varepsilon = 1.3 \times 10^{-3}$ and $\psi = -0.050$, states exhibiting both bimodal and broad peak-height distributions have been observed. Fourth, in addition to these "unimodal" states, states which consist of isolated, high-amplitude peaks ("bimodal" states) are encountered as $|\psi|$ is increased.

The tendency to form strong, isolated peaks culminates in the data in Fig. 10 ($\psi = -0.069$, $c_1 = -0.047$, $c_2 = -5.74$). Here, in strong contrast to the data at smaller $|\psi|$, narrow, stationary peaks coexist indefinitely with the rest of the cell, which remains silent. These are the localized states recently reported by Niemela *et al.* and Anderson and Behringer and explored in detail by our own group.[16] We emphasize that c_1 is close to zero for all of our data. Thus, the qualitative changes seen when we change

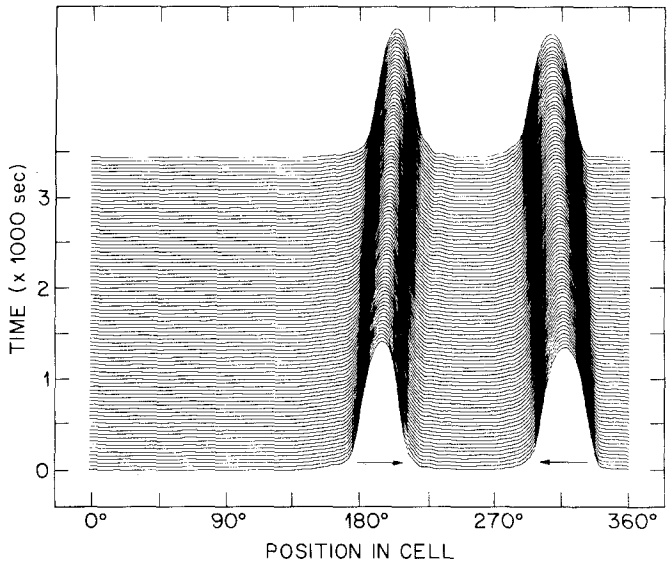

Fig. 10. Spatiotemporal state consisting of two stationary, counterpropagating pulses, at $\varepsilon = 1.0 \times 10^{-3}$, in a fluid with $\psi = -0.069$. In this figure, the total wave amplitude has simply been demodulated in space at each instant in time, so that the left- and right-wave components are not separated. With reduced nonlinear dispersion, narrow, stationary pulses are stable.

ψ are most likely to be caused by the changes in the parameter c_2. For the reduced value $c_2 = -5.74$, the nonlinear dispersion is apparently no longer strong enough to pump wave energy out of the localized pulses, so they do not collapse at $\psi = -0.069$ as they do at smaller $|\psi|$.

We can relate these observations to the computations of ref. 14 by noting that, as we decrease ψ from -0.021 to -0.069, we move the parameters (c_1, c_2) along the solid curve in Fig. 1 of ref. 14, starting near point "*c*" and moving towards point "*d*," Ref. 14 predicts that, as $|c_2|$ drops below about 5 along this curve, bounded chaotic states should no longer be observed. This coincides with our observations, strongly supporting the interpretation that nonlinear dispersion is their cause.

To summarize, weakly nonlinear, one-dimensional traveling-wave convection in an annular container can be modeled by a complex Ginzburg–Landau equation with coefficients that can be accurately measured and calculated. The dynamical states observed in this system consist in the repetitive formation and sudden collapse of narrow pulses. By comparing our results with numerical simulations of the model equation in the parameter limit appropriate to our experiments, and by systematically varying the strength of the coefficient c_2, we can identify strong nonlinear dispersion as the physical effect which is dominantly responsible for our observations.

These observations suggest several new experimental and theoretical directions. We have characterized the observed dynamical states qualitatively by describing the nature of the distribution of pulse heights and the fractions of the system which are "active" or "inactive." An appropriate, quantitative way to statistically characterize these states remains to be implemented, however. We have also not yet begun pursuing another approach to analyzing our data, namely, using the measured wave-amplitude fields to numerically determine which evolution equation the system actually obeys. It may prove possible to deduce the higher-order nonlinearities, as well as the cross-wave coupling, in this way.

On the theoretical side, the first step suggested by these experiments has already been taken: Schöpf and Kramer have shown numerically and analytically that bounded, chaotic solutions of Eq. (1) can exist for $s = 0$ and $g < 0$, provided that $|c_2|$ is large.[14] It would now be of interest to perform a more detailed comparison of these solutions with the experimental observations. In addition, a better theoretical assessment of the higher-order nonlinearities and of the interactions between oppositely-propagating wave components would now be of interest.

ACKNOWLEDGMENTS

We thank W. Schöpf for communicating the results of his calculations to us prior to publications, and many other colleagues for useful discussions.

REFERENCES

1. P. Kolodner, C. M. Surko, and H. Williams, *Physica D* **37**:319 (1989); V. Steinberg, J. Fineberg, E. Moses, and I. Rehberg, *Physica D* **37**:359 (1989).
2. P. Kolodner, D. Bensimon, and C. M. Surko, *Phys. Rev. Lett.* **60**:1723 (1988); D. Bensimon, P. Kolodner, C. M. Surko, H. Williams, and V. Croquette, *J. Fluid Mech.* **217**:441 (1990).
3. P. Kolodner and H. Williams, in *Proceedings of the NATO Advanced Research Workshop on Nonlinear Evolution of Spatio-Temporal Structures in Dissipative Continuous Systems*, F. H. Busse and L. Kramer, eds., NATO Advanced Study Institute, Series B2, Vol. 225 (Plenum Press, New York, 1990), p. 73.
4. D. T. Hurle and E. Jakeman, *J. Fluid Mech.* **47**:667 (1971).
5. P. Kolodner, H. Williams, and C. Moe, *J. Chem. Phys.* **88**:6512 (1988).
6. M. C. Cross, *Phys. Rev. A* **38**:3593 (1988).
7. J. Fineberg, V. Steinberg, and P. Kolodner, *Phys. Rev. A* **41**:5743 (1990).
8. P. Kolodner, J. A. Glazier, and H. Williams, *Phys. Rev. Lett.* **65**:1579 (1990).
9. A. C. Newell, in *Nonlinear Wave Motion*, A. C. Newell, ed. (AMS, Providence, Rhode Island, 1974), p. 157.
10. M. C. Cross and K. Kim, *Phys. Rev. A* **37**:3909 (1988).
11. P. Kolodner, C. M. Surko, and M. C. Cross, unpublished results.
12. W. Schöpf and W. Zimmerman, *Europhys. Lett.* **8**, 41 (1989).
13. C. S. Bretherton and E. A. Spiegel, *Phys. Lett.* **96A**:152 (1983).
14. W. Schöpf and L. Kramer, *Phys. Rev. Lett.* **66**:2316 (1991).
15. C. M. Surko and P. Kolodner, *Phys. Rev. Lett.* **56**:2621 (1986).
16. J. J. Niemela, G. Ahlers, and D. S. Cannell, *Phys. Rev. Lett.* **64**:1365 (1990); K. E. Anderson and R. P. Behringer, *Phys. Lett.* **145A**:323 (1990); P. Kolodner and J. A. Glazier, *Phys. Rev. A* **42**:7504 (1990); J. A. Glazier and P. Kolodner, *Phys. Rev. A* **43**:4269 (1991); P. Kolodner, *Phys. Rev. A* **43**:2827 (1991).